sustainability

MDPI

Article

Sustainable Management of Agro-Food Wastes Derived from the Olive Mill and Sugar Industry and Clinoptilolite to Produce Novel Adsorptive Materials

Christina Megetho Gkaliouri, Zacharias Ioannou *, Nickolas Rigopoulos and Dimitris Sarris

Department of Food Science and Nutrition, School of the Environment, University of the Aegean, Mitrop. Ioakeim 2, 81400 Myrina, Lemnos, Greece; fnsd21008@fns.aegean.gr (C.M.G.); nrigopoulos@aegean.gr (N.R.); dsarris@aegean.gr (D.S.)

* Correspondence: zioan@aegean.gr

Abstract: Novel sorbents were produced using sustainable and eco-friendly methods, aimed at minimizing environmental impact while utilizing industrial by-products and natural minerals. Olive stones and molasses derived from olive mill and sugar industries, respectively, and an abundant, natural and low-cost mineral, clinoptilolite, were combined in the following proportions: 80/20 clinoptilolite/stone, 80/10/10 clinoptilolite/stone/molasses, 50/50 stone/molasses, *w*/*w*. Then, physical carbonization (CL80OL20C, CL80OL10M10C, OL50M50C) or chemical activation (CL80OL20A, CL80OL10M10A, OL50M50A) took place. The adsorbents were characterized through Raman, FT-IR, BET and SEM-EDS analysis. The CL80OL20A material presents the highest ratio of C/O in EDS analysis and the lowest I_D/I_G in Raman spectroscopy. The increase in the specific surface area is as follows: OL50M50C < OL50M50A < CL80OL10M10C < CL80OL20C < CL80OL20A < CL80OL10M10A. Three applications were conducted: two with dyes (methylene blue and methyl red) in aqueous means and one in olive mill wastewaters for the removal of total phenols and their addition to rice, increasing the total phenolic content and producing novel foods. The well-fitted application of the pseudo-second order kinetic model to the experimental data has shown that chemisorption is the prevailing mechanism. The adsorbed amount of the recovered phenols to rice ranges from 0.14 to 0.93 mg/g. Consequently, olive and sugar by-products can be used as filters either to adsorb dangerous organic compounds or to recover bioactive compounds from wastewater, preventing their disposal in the environment, which could otherwise lead to severe negative effects on the ecosystems.

Keywords: olive mill wastewaters; phenol recovery; food enrichment; sugar industry by-products; circular economy; sustainable management

check for updates

Citation: Gkaliouri, C.M.; Ioannou, Z.; Rigopoulos, N.; Sarris, D. Sustainable Management of Agro-Food Wastes Derived from the Olive Mill and Sugar Industry and Clinoptilolite to Produce Novel Adsorptive Materials. *Sustainability* **2024**, *16*, 9204. https://doi.org/10.3390/su16219204

Academic Editor: Ning Yuan

Received: 28 August 2024
Revised: 17 October 2024
Accepted: 21 October 2024
Published: 23 October 2024

Copyright: © 2024 by the authors. Licensee MDPI, Basel, Switzerland. This article is an open access article distributed under the terms and conditions of the Creative Commons Attribution (CC BY) license (https://creativecommons.org/licenses/by/4.0/).

1. Introduction

Olive and olive oil production is one of the main economic pillars of the countries of the Mediterranean basin due to their temperate climate, which favors the growth of olive trees species. In fact, Spain, Italy and Greece are the three leading producers between the countries of the European Union (EU), while Europe is in charge of 70% of the global olive production [1]. In the last few years, the cultivation of olive trees (predominantly species *Olea europaea* L.) has been expanded significantly in other countries as well, due to the rising acknowledgment of the beneficial effects of the bioactive molecules that are contained in olives, such as tocopherol (Vitamin E), phytosterols and flavonoids [1,2]. Nevertheless, parallel to this abundant and rising production of table olives and olive oil, a large amount of waste and by-products are produced as well, primarily olive stones, olive mill wastewater and olive pomace [1]. These residues are characterized by high chemical oxygen demand (up to 200–220 g/L) and biochemical oxygen demand (up to 100 g/L), as well as low pH (4–5) and high phenolic concentration, which render them harmful to the environment and ecosystems, both aqueous and terrestrial [3,4].

Another food industry with wide resonance in the global population is the sugar industry, with a mean production of 160 million tons per year [5]. Sugar, also known as sucrose, can be produced from sugarcane, sugar beet, cassava or other crops with a high content of sugar. These crops thrive in countries with tropical or subtropical climates (e.g., South Africa) [6]. Among them, sugarcane and sugar beet contain the largest amount of sucrose, and thus, they are preferred for cultivation when it comes to industrial purposes [7].

Sugar crystals are covered with molasses, giving them their brown-golden color, which is the original color of raw sugar. The larger amount of raw sugar is used to produce bleached, refined sugar. Sugar production consists of four main steps: crushing sugarcane, juice clarification, crystallization and centrifuge. In each step, different by-products occur. For instance, bagasse after crushing, pressed mud after clarification and molasses after centrifuge [5,7]. Sugar industry wastes, whether solids or wastewater, have negative environmental impacts, especially when they are not properly treated, and they are disposed of in the ecosystem. For example, due to their high organic content and their rapid decomposition, a wide amount of ammonia and heat is generated, which negatively affects plant growth [6]. In addition, sugar-generated effluents adsorb most of the available oxygen from the aquatic ecosystems, leading to death of the organisms that live in it [5].

Organic pollutants such as phenols form the part of effluents of many industries, such as the petrochemical, petroleum refinery, coke-oven, steel foundry, insecticide and herbicide industries [8]. Therefore, its presence is more and more frequent in the bodies of water, and, due to its high toxicity, high oxygen demand and low biodegradability, the phenolic compounds are considered high-priority polluting agents in wastewater treatment [9–14]. The removal of toxic phenolic compounds from wastewater has become a serious environmental concern. Exposure to phenolic compounds may lead to health effects on the brain, digestive system, eyes, heart, kidney, liver, lungs and skin, as well as genetic damages [15,16].

Different treatment methods have been applied to remove organic compounds from wastewater, such as biological treatment, catalytic wet oxidation, photochemical treatment, solvent extraction, incineration, reverse osmosis and adsorption [16,17]. Adsorption technology presents a lot of benefits in comparison to other methodologies such as effectiveness and simplicity in its application. The adsorption of organics onto activated carbon has been studied in the past, and the results demonstrated that the adsorption behaviors depend mainly on the characteristics of the activated carbon, the molecular properties of the organics and the operational conditions. The characteristics of the activated carbon such as surface area, pore size distribution and surface functional groups play an important role in adsorption, as they determine the interactions between the organics and the activated carbon at the interface [18,19].

Plant biomass represents one of the most abundant and underutilized biological resources on the planet and is seen as a promising source of material for fuels and precursors for activated carbon production [11]. Low-cost materials such as biomass and waste materials are a renewable and inexpensive additional source of activated carbons. Typical waste includes peach stones [20], olive stones [21], palm kernel shells [22], *Arundo donax Linn* and pomelo peel [23], coconut shell [24], corn stalks [25], waste macadamia [26], apple peels [27], rice husks [28], almond shells and apricot stones [29], yellow mombin fruit stone [30], pristine gelatin and starch [31], radish press cake [32] and bamboo waste [33,34]. The conversion of such materials to activated carbons leads to the reduced cost of waste disposal, increases their financial value and provides an inexpensive alternative to the existing commercial activated carbons [35].

Carbonization is the process of the thermal degradation of raw materials at temperatures ranging between 300 °C and 1100 °C [36,37] in an inert atmosphere, e.g., under nitrogen or argon gas flow [36,38]. During the carbonization process, a primary porosity network is formed [39]. It is widely accepted that biomass pyrolysis consists of three main stages over the whole temperature range, which are moisture elimination and drying of the material (first stage), consecutive minor devolatilization and major degradation of the

more unstable polymers (second stage) and the decomposition of a high-stability structure (third stage) [37]. The degradation of lignocellulosic materials during carbonization usually follows the following order during temperature scaling: hemicellulose degrades at temperatures ranging between 200 and 350 °C and cellulose at 200 and 500 °C, while lignin is characterized by a slower decomposition rate and its degradation takes place in a wider temperature range, more specifically, between 150 °C and 900 °C [40]. Carbonization and pyrolysis use the heating of the material in an inert atmosphere (absence of air). Carbonization is used for the increase of carbon content in the initial raw material [41] but pyrolysis is needed for the extraction of other products like char, volatile organic compounds, etc.

During the activation process, which acts complementary to carbonization, or it can also be performed regardless of it, the existing pores are further developed while parallel new pores are created as well. Thus, the specific area of the materials and the pore volume are improved through activation and a well-constructed pore network is finally settled. Therefore, the activation stage is considered to be the most crucial and affects most of the properties of the formed adsorbent [37]. There are mainly three different processes of activation: physical activation, chemical activation and physio–chemical. Among them, chemical activation seems to form adsorbents with better characteristics and higher performance. The principal factors that influence the process of chemical activation include, among others, the type of activating agent, the mixing method, the mass ratio of activating agent to carbon precursor, and the heating method as well [42]. Regarding the type of activating reagent, these are clustered into four groups depending on their acid–basic behavior: acidic, neutral, alkaline, and self-activating agents. Different activating reagents tend to react with different polymers (e.g., lignin, cellulose etc.) [37].

Zeolites are hydrated aluminosilicates containing cations in their structure, such as sodium or potassium, and other monovalent or multivalent metals such as calcium and magnesium [43]. Their basic structure consists of a three-dimensional tetrahedral framework of $(SiO_4)^{4+}$ and $(AlO_4)^{5+}$, where each oxygen is shared by two tetrahedra. They present high porosity and ion exchange capacity and so are ideal as adsorptive materials [44]. Clinoptilolite is one of the most abundant zeolites, with a Si/Al ratio equal to 2.1 up to 5.3, leading to a stable mineral under high temperatures and acidic conditions. Due to its unique properties, such as low cost, high surface area, recyclability, high cation exchange capacity and wide distribution, it can be utilized in different sectors, from agriculture and industry to medicine [45].

The aim of this current research was to make good use of agro-food industry by-products that are discharged in the ecosystem, leading to negative effects, via using methods that promote sustainability. The conversion of these materials in adsorbents, either through carbonization or chemical modification, and their characterization through FTIR, Raman, BET and SEM-EDS analysis, has resulted in multiple applications that contribute to the elimination of various pollutants, such as synthetic dyes and phenols. On the other hand, phenolic compounds in the human diet can promote health and well-being. Therefore, reclaiming these molecules from agro-industrial sewage (e.g., olive mill wastewater) to enrich food such as rice can favor both the environment and human health as well.

2. Materials and Methods

2.1. Materials

Solid wastes, especially olive stones of the Greek olive mill industry, were used in the production of adsorbents. Sugarcane molasses (Fytro, Athens, Greece) was obtained from the local market. The clinoptilolite used in this present study came from S&B company [46]. Methylene blue and methyl red dyes were bought from Merck Industry in Greece.

In the olive oil industry, olive stones are collected, washed to eliminate any residual oil, dried and finally crushed into various sizes. In this experiment, ground olive stones and clinoptilolite in standard powder form (100–500 μm) were sieved up to 300 μm. Then, clinoptilolite, olive stone and molasses were mixed in different proportions: 80/20 *w*/*w* zeolite (CL)/olive stone (OL), 80/10/10 *w*/*w* zeolite (C)/olive stone (OL)/molasses (M)

and 50/50 *w*/*w* olive stone (OL)/molasses (M). Moisture content of the three mixtures was determined according to ISO 11465/1993 [47]. Moreover, for the determination of ash, samples were subjected to dry ashing according to John and Case, 1990 [38,48]. Volatile matter was determined according to the European Standard EN15148-2009 [49]. Fixed carbon content was later estimated by the difference. Elemental analysis was executed using a Perkin Elmer 2400 CHN elemental analyzer using a combustion method to convert the sample elements to simple gases (CO_2, H_2O, N_2). The product gases were measured as a function of thermal conductivity. Then, the specimens either followed a carbonization process or a chemical activation process. The initial mass of the samples was 3.9 g for olive stone and molasses (50/50 *w*/*w*) and 5.0 g for each of the rest materials. The samples were placed in ceramic crucibles in a horizontal pyrolysis oven with a continuous flow of nitrogen (500 mL/min). The carbonization program consists of the following steps: there is an increase of the temperature up to 200 °C with an increasing temperature rate of 10 °C/min; it remains stable for 10 min, heats up until 400 °C with the same rate and then remains stable for 10 min; and, finally, there is an increase of temperature up to 650 °C with 10 °C/min, the temperature remains stable for 10 min, heats up until 900 °C with a temperature range of 10 °C/min, and remains stable there for 10 min. The carbonaceous materials were weighed before and after the carbonization process. The chemical activation (A) of the specimens includes the impregnation of 2.5 g of each one in a solution of 20 mL of HCL acid 6 M for 1 day under stirring up to 170 rpm. The purpose of this experiment was to use a strong acid such as HCL or H_2SO_4. Since we have not previously conducted an activation process where a weak acid would be necessary for the increase of pores such as H_3PO_4, it was necessary to use an acid like HCL in a middle concentration—for instance, 6 M—to create the necessary pore structure in the materials. High concentration of acid such as 12 or 18 M will destroy the pore structure of the materials [50,51]. Moreover, it is necessary to create the appropriate conditions for good contact between the acid and the lignocellulosic material. For this reason, it is necessary to impregnate the lignocellulosic material to the solution (20 mL) and to stay there for the appropriate time (1 d) to react the acid with the material. Other researchers proposed the same period with the same reaction agent [50]. To examine the best contact time between the samples and HCL acid, we impregnated each one (CL80OL20A, CL80OL10M10A, OL50M50A) to HCL of 6 M for 12 h and 48 h, and then we conducted MB adsorption experiments. The results showed that the adsorption in equilibrium was reached at higher time intervals in comparison with the materials impregnated to HCL in 1 d; i.e., the materials reached an equilibrium after 10–15 min when impregnated in HCL 6 M for 12 h and after 20–30 min when impregnated in HCL 6 M after 48 h. The specimens were then removed from the solution, rinsed with deionized water until the pH of the filtrate became neutral and were finally dried in an oven at 105 °C for 24 h to obtain a stable final weight according to the literature [52–54]. The final carbonized products were characterized as CL80OL20C, CL80OL10M10C and OL50M50C for the proportion of 80/20 CL/OL, 80/10/10 C/OL/M and 50/50 OL/M *w*/*w*, respectively. The chemically activated materials were mentioned as CL80OL20A, CL80OL10M10A and OL50M50A for the proportion of 80/20 CL/OL, 80/10/10 CL/OL/M and 50/50 OL/M *w*/*w*, respectively.

2.2. Characterization of the Adsorbents

An Agilent Cary 630 FTIR spectroscope, equipped with an ATR accessory, was used with Microlab Pharma 5.8 software. All measurements were performed on the same day at 25 °C. The spectra were measured in the region from 400 to 4000 cm^{-1}. The diamond ATR sensor was cleaned with ethyl alcohol or acetone before each sample measurement.

The SEM-EDS studies of the adsorbents were carried out in a JEOL JSM-IT500 Scanning Electron Microscopy (SEM), JEOL Ltd., Boston, MA, USA and simultaneously, elementary analysis was determined by Energy Dispersive X-Ray Spectrometry (EDS) with the use of an x-Act detector from Oxford Instruments, High Wicombe, UK. The 108C Auto Carbon

Coater is the advanced sample coater available for coating non-conductive specimens prior to SEM X-Ray analysis.

The micro-Raman spectra were obtained using an inVia Qontor Renishaw Raman device Renishaw UK Ltd., Gloucestershire, UK, equipped with a microscope and a CCD detector. As a source of excitation, a diode laser with a radiant emission wavelength of $\lambda = 785$ nm was used. The beam size of the laser is of the order of ~1 μm. The power density on the surface of the sample was ~1 mW/μm^2 and the spectral resolution was ~4 cm^{-1}. Alignment and calibration of the spectrometer, before and after each measurement, were achieved using crystalline silicon (Si) wafer adapted within the Raman device.

The specific surface area and the porosity of the adsorbents were analyzed with the use of the Tristar II plus surface area and porosity analyzer. The carrier gases were helium and nitrogen. Samples were weighed, placed in a sample container on the analyzer and degassed individually for 24 h at 400 °C. The weight of the samples ranges from 0.1 to 0.3 g. More specifically, the sample weights were 0.3 g for CL80OL20C, 0.3 g for CL80OL10M10C, 0.2 g for OL50M50C, 0.1 g for CL80OL20A, 0.1 g for CL80OL10M10A and 0.1 g for OL50M50A. They were then allowed to cool before being stored under nitrogen gas at a pressure of 5 mmHg for 24 h. Characterization in terms of specific surface area, pore volume and pore diameter of the obtained materials was determined by N_2 adsorption–desorption at −196 °C using the BET method. The micropore volume was calculated by using t-Plot micropore volume. The pore size distribution was determined by using the Barrett–Joyner–Halenda (BJH) model [55].

2.3. Applications of the Adsorbents

The materials were tested for their adsorptive properties using either different dye aquatic solutions or olive mill wastewater.

Two different dye aquatic solutions were prepared in a concentration of 0.032 g/L as studied previously [56,57]. The first one contains the cationic methylene blue dye, and the second one the anionic methyl red dye. More specifically, 0.14 g of each adsorbent was mixed with 14 mL of dye and placed in test tubes in a proportion of 10 g of adsorbent/L of dye. Then, the samples were stirred at 240 rpm and 25 °C, and at different time intervals, an amount was taken and centrifuged for 5 min at 5000 rpm. The absorbance of each sample was measured in the visible spectrophotometer ONDA V-10 Plus spectrophotometer ($\lambda = 664$ nm for MB and $\lambda = 419$ nm for MR) [58]. The whole procedure lasts until the adsorption reached equilibrium. The above procedure was repeated three times for each sample.

The adsorptive ability of the samples was also examined in the removal of phenolic compounds from olive mill wastewater (OMWW). OMWW samples were collected during the oil-harvesting season from an olive mill located in the island of Lemnos (Greece). Samples were collected in PTFE plastic bottles and transported to the laboratory immediately after sampling and stored at 4 °C. Subsequently, filtration was performed to remove any solid particles from wastewater. The adsorption experiment procedure was followed: 0.1 g of each adsorbent was mixed with 10 mL of olive mill wastewater and placed in test tubes in a proportion of 10 g of adsorbent/L of wastewater. Then, the samples were stirred and centrifuged for 5 min at 5000 rpm. Thereafter, the concentration of the remaining phenolics in the supernatant of each sample was tested following the Folin Ciocalteu protocol [59]. The absorbance of each sample was measured in the spectrophotometer ($\lambda = 765$ nm). The above procedure was repeated three times for each sample. The adsorbed amount (q_t) of the adsorbate onto the adsorbent was determined from the difference between the initial amount of adsorbate (q_o) in the solution and the measured amount of the adsorbate. Then, the materials were dried at 40 °C for 24 h and weighed. Studies have shown that the decomposition of certain phenolic compounds can increase with rising temperatures, with some compounds becoming less stable over time. More specifically, phenolic compounds that are present in olive oil and thus in olive mill wastewater (e.g., tyrosol) are stable in temperatures that do not exceed 50 °C [60]. The time period was 24 h because

this time was enough to receive a dry sample without losing phenolic compounds. This temperature/time combination has also been used by other studies as well [61].

The dried materials were inserted into falcon tubes with deionized water in a proportion of 0.1 g of adsorbent/10 mL of solution, stirred and centrifuged at 170 rpm at different time intervals. After that, the solutions were filtered to remove the adsorbents, and the supernatant was added to falcon tubes with rice in a proportion of 0.1 g of rice /mL of supernatant. The above procedure was repeated three times for each sample. The concentration of the desorbed phenolic compounds in the supernatant of each sample was tested following the Folin Ciocalteu protocol [59]. The adsorbed amount (q_t) of phenolic compounds onto the rice was determined from the difference between the initial quantity of phenolic compounds (q_o) in the solution and the measured quantity of phenolic compounds in the solution at different time intervals.

3. Results and Discussion

3.1. RAMAN, FTIR, SEM-EDS and BET Characterization of the Adsorbents

Table 1 gives the results for the moisture, proximate and ultimate analyses of the samples. The amount of S and CL was calculated according to the rule of mixtures from the values of olive stone and molasses obtained from the literature [62,63]. The values obtained clearly indicate the different quality levels of these three samples. The CL80OL20 sample has similar moisture, ash and volatile values as those of the CL80OL10M10. The olive stone sample (OL50M50) presents the highest moisture, volatile matter and fixed carbon and the lowest ash content compared to the other two samples, due to the lack of clinoptilolite. According to the literature [64], the TG-DSC curves of clinoptilolite show a small, single and broad endothermic peak from 120 °C or 140 °C up to 680 °C or 800 °C according to the origin of clinoptilolite. The mass loss ranges from 9.48 to 9.87% [64]. The endothermal effects are attributed to the dehydration of the zeolite minerals. Consequently, the total structural decomposition of the clinoptilolite occurs at temperatures over 1000 °C [64]. Moreover, the elemental analysis has shown that OL50M50 presents the highest percentage of C, H and N compared to the other samples due to the lack of C and N in clinoptilolite. The general formula of clinoptilolite is as follows: $(K, Na, Ca)_6[(Si, Al)_{36}O_{72}]\ nH_2O$ (n = 20–24) [64]. Comparing olive stone and molasses from the literature [62,63], it seems that molasses appears to have a higher amount of N, S and CL and a lower amount of C compared to olive stones. Moreover, molasses and olive stones appear to have other elements such as oxygen, potassium, sodium, calcium, magnesium, iron, phosphorus, aluminum and silicon. The highest percentage of the above elements belongs to oxygen, i.e., 41.97 wt% in db in olive stone and 42.60 wt% in db in molasses [62,63]. The high VM content of molasses is most likely because it is mainly composed of low-molecular weight organics, such as sugars [63]. Molasses has a higher FC content compared to olive stones, suggesting that it may yield more CO gas than the rest of the fuels during gasification [63]. The same behavior also happens when comparing the FC values of CL80OL20 and CL80OL10M10. Olive stone and CL80OL20 samples have a rather low S value compared to molasses and CL80OL10M10 samples, indicating low SO_2 emissions [62].

Table 1. Moisture content (wt%, wet basis), proximate analysis results (wt%, db) and elemental composition (wt%, db) of the mixtures (CL80OL20, CL80OL10M10, OL50M50) and raw materials (olive stone and molasses).

Sample	Moisture	ASM	VM	FC	C	H	N	S	CL
CL80OL20	6.80	75.01	22.95	2.04	9.81	1.98	0.46	0.06×10^{-1}	0.05×10^{-1}
CL80OL10M10	7.07	74.04	21.66	4.30	9.06	1.71	0.25	0.14	0.28
OL50M50	11.06	4.53	72.04	23.43	48.62	7.81	1.14	0.72	1.41
Olive stone *1	11.20	1.20	78.70	20.10	50.35	5.95	0.34	0.03	0.25×10^{-1}
Molasses *2	13.00	19.00	53.00	28.00	37.90	5.20	0.50	1.40	2.80

*1 According to Castells et al., 2023 [63]. *2 According to Dirbeba et al., 2021 [62].

The weight loss percentage of each carbonaceous material, i.e., CL80OL20C, CL80OL10M10C, OL50M50C and commercial zeolite is presented in Figure 1. The OL50M50C sample presents the highest weight loss percentage (75.2%), while CL80OL10M10C presents the lowest (27.2%). CL80OL20C presents intermediate values (28.2%). All carbonaceous materials were compared to commercial zeolite (Z), which also undergoes the same thermal process. The weight loss decreases in the materials in the following order: OL50M50C > CL80OL20C > CL80OL10M10C > Z, respectively. Zeolite as a mineral presents the lowest weight loss due to the evaporation of water molecules (free and crystalline water) [65]. Zeolites and, more specifically, clinoptilolite are used as the matrix/template for the development of the additional structure of carbons derived from olive stone and molasses (CL80OL20C, CL80OL10M10C, OL50M50C) or the chemically modified structure of olive stones and molasses (CL80OL20A, CL80OL10M10A, OL50M50A). Consequently, a high amount of zeolite is needed compared to olive stone and molasses. Moreover, another basic aspect is the effect of olive stone or molasses or both in the final carbonaceous or chemically modified product. As a result, we proposed the production of three materials, i.e., 80/20 *w*/*w* zeolite(CL)/olive stone(OL), 80/10/10 *w*/*w* zeolite (C)/olive stone (OL)/molasses (M) and 50/50 *w*/*w* olive stone (OL)/molasses (M). The proportion of the last material indicates the need to comprehend the behavior of the final products, i.e., carbonaceous or chemically modified, without the presence of zeolites.

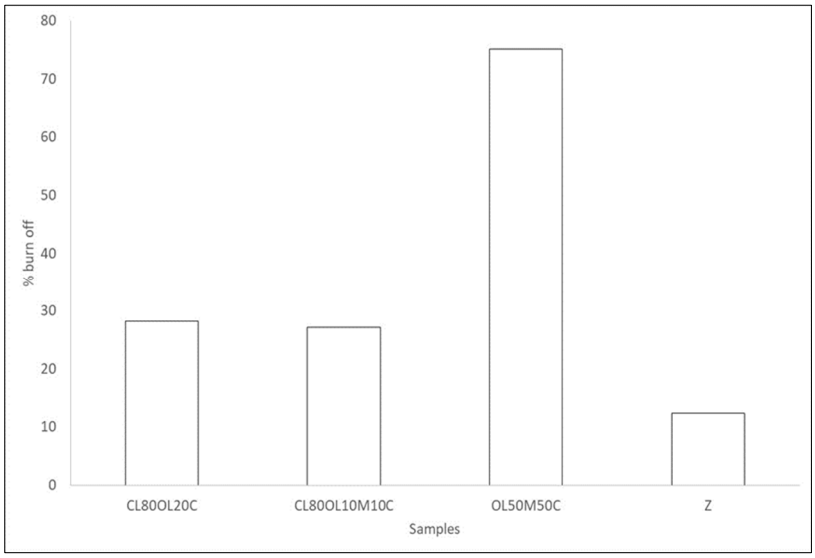


Figure 1. Weight loss percentage of the carbonaceous materials in regard to carbonized commercial pure zeolite.

Raman spectra for the adsorbents and, more specifically, the carbon structures that were developed in the zeolitic template exhibit mainly two bands at 1600 and 1330–1350 cm^{-1}, the former band being called the graphite band (G band) and the latter the defect-induced band (D band) (Figure 2).

The G band represents stretching vibrations with the basal graphene layers. The width of the G band is correlated with the stacking ordering between the adjacent graphene layers. The D band is related to disorder and is not present in pure graphite [66,67]. Its intensity is strictly connected to the presence of six-fold aromatic rings [68]. The carbonaceous adsorbents show inhomogeneity according to the optical microscope of the Raman system. Raman spectra also present bands at approximately 215, 397, 488 and 590 cm^{-1}. According to the literature [69], these bands correspond to zeolite Raman signals. Consequently, except for the main Raman spectra, other absorption wavenumbers, especially in the CL80OL10M10C sample, are presented due to the appearance of traces of elements such as CaO at 280 cm^{-1}. As is evident from Figure 2, the Raman spectra show a distinct increase in the intensity narrowing of the width of the 1330 cm^{-1} band compared to the

1600 cm^{-1} band. The ratio between the peak intensities of the G and D bands (the so-called I_D/I_G ratio) is a useful indicator of the sample crystallinity [70]. The lower the I_D/I_G values, the higher the crystallinity will be. The values of I_D/I_G ratios follow the order of CL80OL20C (1.22) < CL80OL10M10C (1.25) < OL50M50C (3.74). The observed I_D/I_G ratios for CL80OL20C, CL80OL10M10C and OL50M50C are typical for amorphous carbon materials [71].

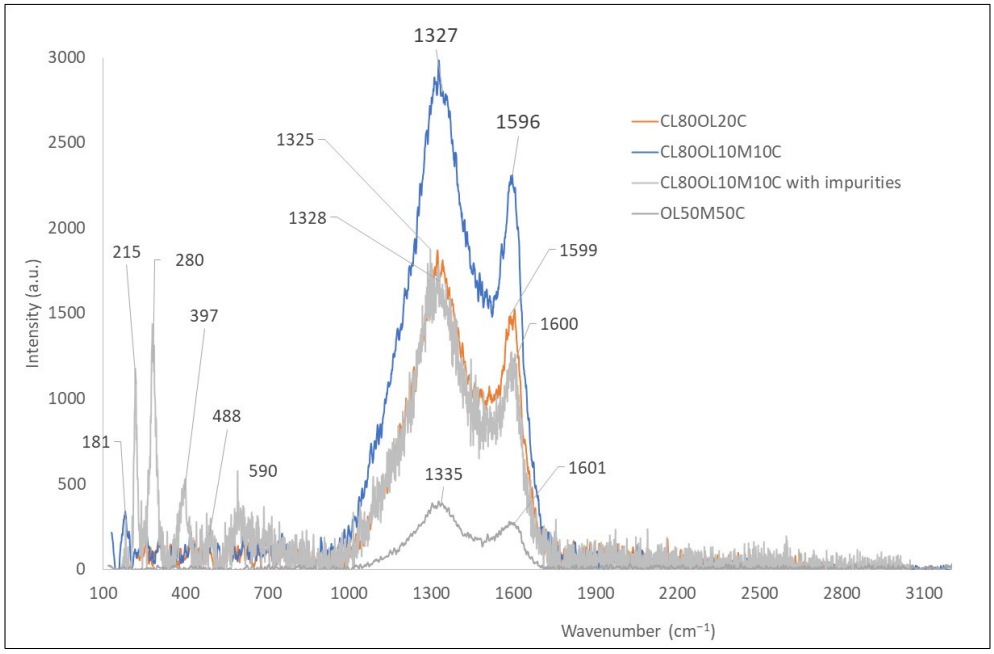


Figure 2. Raman spectra of carbonaceous adsorbents.

As it is known, the G band results from the optical zone center phonon of E_{2g} symmetry, while the D band is related to a disorder-induced mode resulting from a zone boundary phonon of A_{1g} symmetry [72,73]. The ratio of the D band intensity versus the G band intensity is an indicator of the sp^3 content in carbons. The carbonaceous materials present a mixed structured of sp^2 and sp^3 carbon. A decrease in the I_D/I_G rato indicates a decrease in the number of sp^3 atomic sites in activated carbon, and such materials are more graphite-like [72]. According to the I_D/I_G ratio of carbonaceous materials, the CL80OL20C adsorbent presents the lowest I_D/I_G in all the produced adsorbents, having more sp^2 atomic sites, and is a more graphite-like material. The definition of graphitic carbons consists of the carbon atoms that are three-coordinated and are bound by sp^2-type hybrid orbitals [74]. According to the literature [74], highly disordered carbons such as charcoal and coke have very broad bands, as presented in Figure 2, whereas the lines are narrower in glassy carbon and polycrystalline graphite. The chemically activated materials CL80OL20A, CL80OL10M10A and OL50M50A do not show Raman peaks due to their different preparation compared to carbonaceous ones.

A basic target of this present study is the comparison between the carbonization and chemical modification methods. This comparison is achieved by studying the properties and applications of the final carbonaceous or chemically modified materials. Key elements that are studied are the chemical groups developed through FTIR analysis, morphological imaging and elemental analysis through SEM-EDS analysis; the specific surface area and the porous network through BET analysis; and, finally, an examination of the behavior of the final products in various applications. All the above justifies the production of either individually carbonized or chemically modified materials, but in no case justify the use of carbonaceous and then chemically modified materials.

The FTIR spectra of carbonaceous and chemically modified materials are presented in Figure 3. All materials show a strong absorption band at 1010–1030 cm^{-1}, which

corresponds to bending vibrations "in plane" of C–H or to Si–O in tetrahedral sheets of zeolite [75,76]. The spectrum of OL50M50A presents two weak bands at 2929 and 2873 cm^{-1}, which correspond to –C–H vibrations (such as $–CH_2–$ groups). Moreover, a weak band at 790 cm^{-1} was assigned to out-of-plane alkene (=C–H) bending or the out-of-plane bending of ring C–H bonds. Finally, the absorption bands at 600–610 cm^{-1} correspond to the Si–O–AL bending vibrations of clinoptilolite [76]. Other studies of synthetic materials [77] have shown similar results, indicating that the bands at 1046.25 cm^{-1} were assigned to the framework stretching vibration band of Si (Al)–O, and 2920.149 and 2856.403 cm^{-1} indicate C–H aliphatic stretching and $–O–CH_3$ of the aldehyde group [77]. The FTIR analysis of commercial activated carbons [78] such as coal-derived granular-activated carbons, coal-derived powdered activated carbons and coconut shell-derived powdered activated carbons has proven the presence of C–H stretching of $–CH_3$, $–CH_2$ groups and C=O stretching. Most of the above absorption bands are weak, especially for carbons, showing that the presence of many groups was difficult to identify due to their low concentration and proportion in comparison with the element of carbon and due to the spectrum background, which is caused by the absorption of the black color of carbonaceous materials [54].

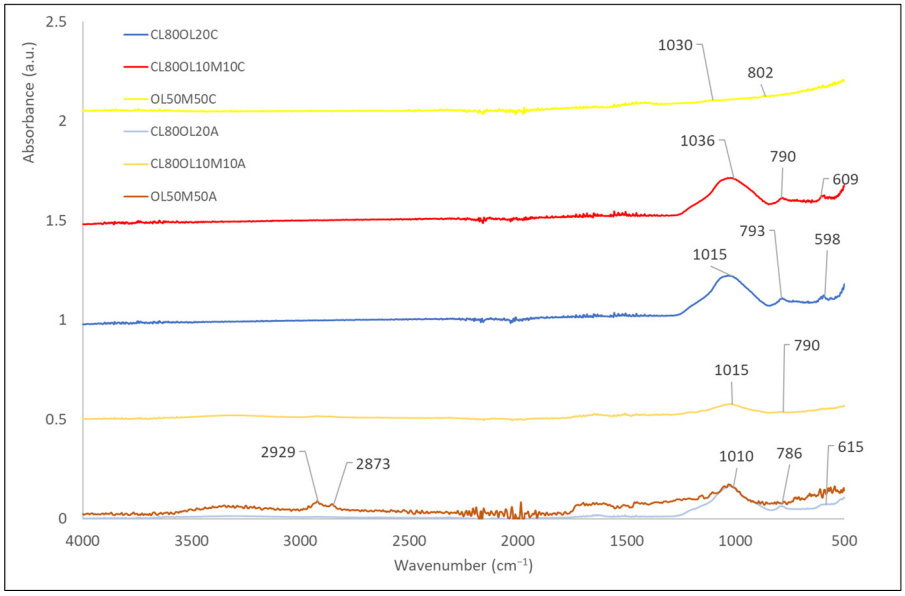


Figure 3. FTIR spectra of carbonaceous and chemically modified materials.

Scanning electron microscopy with EDS analysis is also presented for the six different materials (Figure 4). SEM images are included in two magnifications, i.e., 1000× and 500×, for carbonaceous and chemically modified materials. Comparing carbonaceous materials CL80OL20C, CL80OL10M10C and OL50M50C with chemically modified CL80OL20A, CL80OL10M10A and OL50M50A, it seems that the latter show well-formed pore structures with the corresponding free passages between the particles. Moreover, the materials OL50M50C and OL50M50A, which contain molasses and olive stone, present more compact structures with fewer free passages compared to the rest of the materials, in which clinoptilolite prevails. SEM images of commercial activated carbons such as coal-derived granular activated carbons, coal-derived powdered activated carbons and coconut shell-derived powdered activated carbons have proven either the presence of a skeletal structure with pores or a uniform morphology, while cavities in the activated carbon structure are favorable for the adsorption process [78].

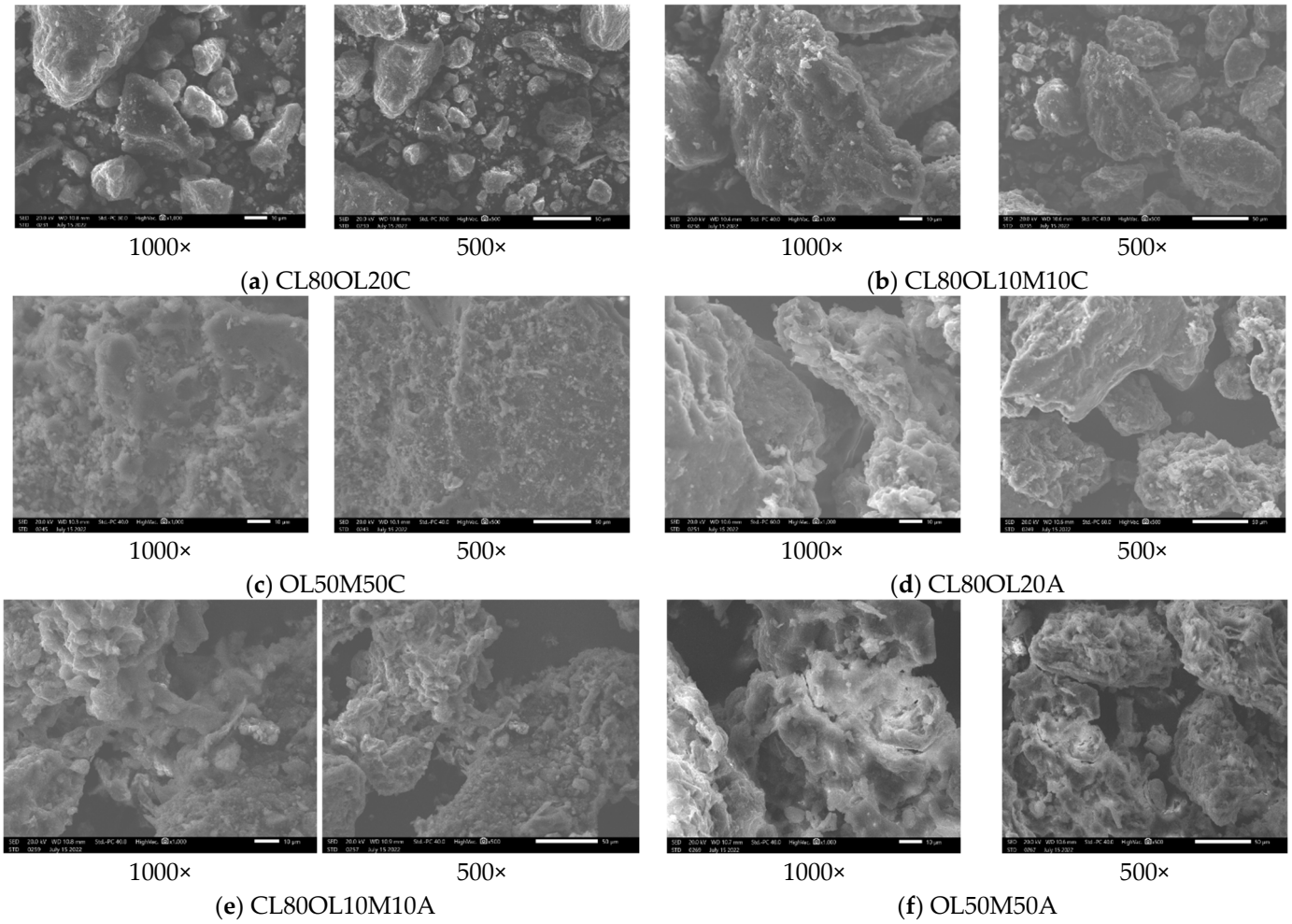


Figure 4. Scanning electron microscopy of the six materials in two different magnifications 1000× and 500×. Scale bar = 10 μm and 50 μm.

Based on the EDS analysis (Table 2), the main elements are carbon from 67.8 up to 89.9% and oxygen from 9.4 up to 30.6% for all materials. Carbonized adsorbents CL80OL20C, CL80OL10M10C and OL50M50C appear at a higher concentration of carbon and a lower concentration of oxygen compared to those that are chemically modified, i.e., CL80OL20A, CL80OL10M10A and OL50M50A, due to the carbonization process. Comparing CL80OL20C with CL80OL10M10C and OL50M50C, it seems that it contains the highest amount of carbon (90%) and the lowest amount of oxygen (10%), presenting similarities with commercial activated carbon [54]. The increase in the ratio of C/O for all the materials follow the order CL80OL20A < CL80OL10M10A < OL50M50A < CL80OL10M10C < OL50M50C < CL80OL20C. The samples contain other elements, such as Si and Al, the main components of the zeolitic structure. Moreover, the zeolitic structure also contains exchange cations such as Na, K, Ca and Mg, which are included in low percentages in CL80OL20C, CL80OL10M10C, OL50M50C and CL80OL10M10A materials [79]. According to Table 2, the presence of K, Ca, Mg, Na, P and S in the materials may also be explained by the fertilizers used during the agriculture of olive trees [54] and presented strongly in CL80OL10M10C and CL80OL10M10A materials, with the highest content of olive stone (10%). Finally, molasses contains not only total carbohydrates, reducing sugars, protein, fat and moisture but also potassium, sodium, phosphorus, magnesium and calcium, which are basic elements in the adsorbents with the highest amount of molasses, i.e., OL50M50C [80]. Other studies [77] have shown the presence of C (28.01%), O (50.96%), Si (9.27%), Al (1.55%),

Na (2.20%), K (1.26%) and Ca (6.57%) during the formation of activated carbon/zeolite nanoparticles that were used for the adsorption of MB.

Table 2. EDS analysis (*w*/*w*) of the carbonaceous and chemically modified materials.

Samples	C	O	Si	Ca	Al	Mg	K	Na	P	S	C/O
CL80OL20C	89.9	9.4	0.3	0.2	0.1	0.1	-	-	-	-	9.6
CL80OL10M10C	75.7	21.2	1.4	0.6	0.3	0.1	0.2	0.1	0.4	-	3.6
OL50M50C	74.9	10.0	0.3	4.5	-	0.4	8.3	0.4	0.4	0.8	7.5
CL80OL20A	67.8	30.6	1.0	-	-	-	-	-	-	0.6	2.2
CL80OL10M10A	73.8	25.8	0.3	-	0.1	-	-	-	-	-	2.9
OL50M50A	73.0	22.4	0.6	2.4	-	-	-	-	-	1.6	3.3

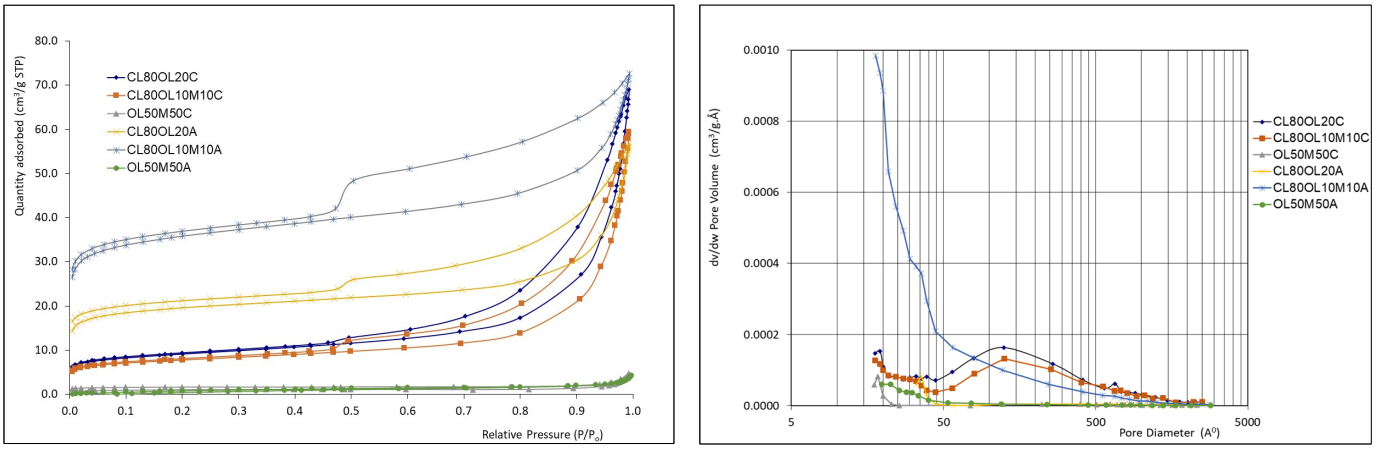
Comparing Tables 2 and 3, it seems that the highest specific surface area is presented in adsorbents with the lowest content of carbon and the highest content of oxygen (CL80OL20A, CL80OL10M10A). Similar results are mentioned elsewhere [81]. Initially, the materials present a dense structure with a low specific surface area and pore volume. After carbonization or chemical modification, the materials increase the pore structure, which is occupied by disordered carbon and oxygen-containing functional groups. Then, some oxygen-containing functional groups react with carbon materials producing gases such as CO, CO_2 and water vapor. The influence of oxygen-containing functional groups increases significantly in the lowest pore diameters of the materials. Kim et al. (2019) [82] reported that carbonyl groups are responsible for the increase in the specific surface area of carbons, whereas the presence of carboxyl groups decreases the specific surface area of carbons. In general, the chemical activation of carbon materials increases oxygen-containing functional groups [83]. These functional groups form chemical bonds through electrostatic interactions, leading to various adsorbent applications [84].

Table 3. Characteristics of pore structure, i.e., S_{BET}: specific surface area, V_{tot}: total pore volume, V_{micro}: micropore volume, $d_{aver.p.d.}$: adsorption average pore diameter, $d_{BJH,\ aver.p.d.}$: BJH adsorption average pore diameter.

Samples	S_{BET} (m^2/g)	V_{tot} (cm^3/g)	V_{micro} (cm^3/g)	$d_{aver.p.d.}$ (Å)	$d_{BJH\ aver.p.d.}$ (Å)
CL80OL20C	33.12	10.68×10^{-2}	0.60×10^{-2}	128.99	210.82
CL80OL10M10C	28.12	9.14×10^{-2}	0.54×10^{-2}	130.03	228.73
OL50M50C	3.88	0.73×10^{-2}	0.05×10^{-2}	175.32	256.59
CL80OL20A	73.89	8.79×10^{-2}	2.00×10^{-2}	47.59	142.21
CL80OL10M10A	135.32	11.23×10^{-2}	3.66×10^{-2}	33.22	86.28
OL50M50A	4.17	0.67×10^{-2}	0.12×10^{-2}	64.11	95.58

The basic characteristics of the pore structure of all adsorbents are given in Table 3. Comparing the specific surface area (S_{bet}) of the materials, it seems that the increase in the S_{bet} follows the order OL50M50C < OL50M50A< CL80OL10M10C < CL80OL20C < CL80OL20A < CL80OL10M10A. Comparing the carbonaceous and chemically modified adsorbents with the same proportion of raw materials, e.g., CL80OL20C-CL80OL20A, CL80OL10M10C-CL80OL10M10A and OL50M50C-OL50M50A, it seems that the chemical activation process gave significantly higher specific surface area to the materials compared to the carbonization process. In accordance with the classification adopted by the International Union of Pure and Applied Chemistry (IUPAC) [85], the adsorbent pores are classified into three groups: micropore (diameter < 2 nm), mesopore (2–50 nm) and macropore (>50 nm). The adsorption average pore width according to the BET and BJH methods shows that all materials mainly exhibit pores of diameter in the range of 3–25 nm, in which the pore sizes become predominantly mesoporous. The porous features of the adsorbents are analyzed using nitrogen isothermal adsorption/desorption measurements and pore

size distributions (Figure 5). All samples show a type IV isotherm with a hysteresis loop, indicating mesopore structures. The hysteresis loops of type H3 are characteristic of the mesoporous material with slit-shape pores or wedge-shaped pores according to IUPAC classification [86] and monolayer formation, which begins at low pressures, and multilayer formation occurs at medium pressure. The pore size distribution measurements (Figure 5b) also show that the addition of zeolite in the mixture of molasses and olive stone increases the mesopore structure of the material, i.e., CL80OL20C, CL80OL10M10C, CL80OL20A and CL80OL10M10A compared to OL50M50C and OL50M50A [87]. Other studies have shown that the use of coal gangue-based zeolite granules in a fluidized bed confirmed that the synthetic zeolite was microporous, with a pore size of 0.44–1.89 nm, and the specific surface area, pore volume and average pore size of the synthesized zeolites were determined by BET analysis to be 518.7 m^2/g, 0.243 cm^3/g and 1.61 nm, respectively [88]. Commercial activated carbons [78], i.e., coal-derived granular activated carbons, coal-derived powdered activated carbons and coconut shell-derived powdered activated carbons, showed high surface areas of 700.57 m^2/g, 542.33 m^2/g and 1025.02 m^2/g, respectively. The adsorption isotherms of them presented a mixture of type I and type IV isotherms, while the average pore sizes were 2.22, 3.25 and 5.01 nm, respectively. Commercial activated carbons were derived primarily from soft or hard wood; soft, semi-hard or hard coal; and petroleum coke [10], indicating that the raw materials come from fossil fuels and wood and not from agricultural by-products.

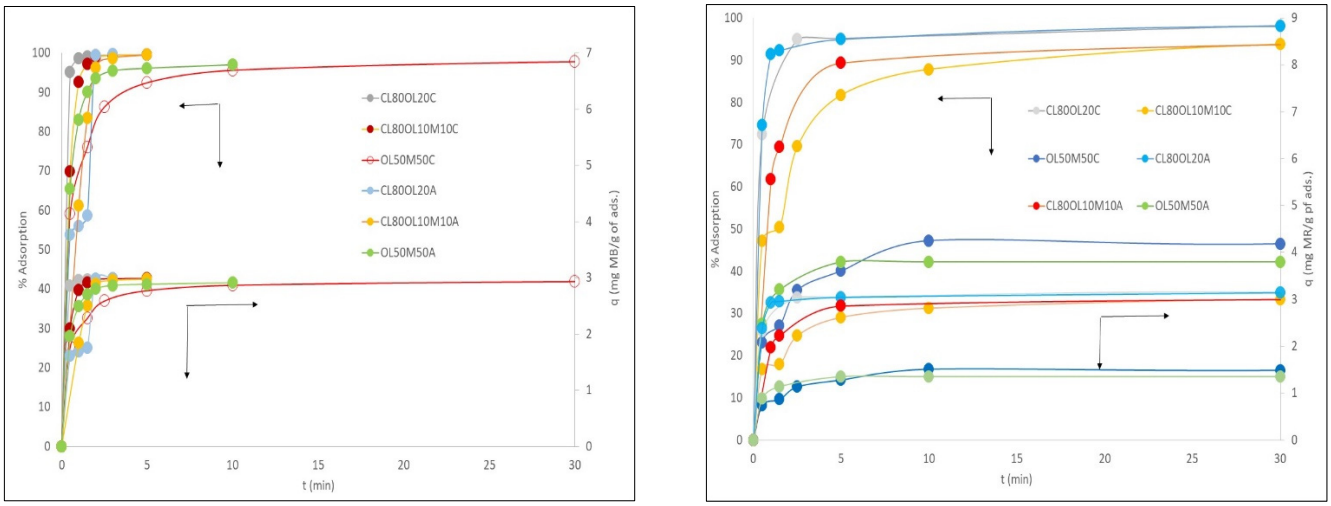


(**a**) (**b**)

Figure 5. (**a**) The N_2 adsorption−desorption isotherm and (**b**) the pore size distribution (PSD) based on the BJH method of the prepared samples.

3.2. Environmental and Food Applications of the Adsorbents

Three different batch experiments were conducted to study the behavior of the carbonized and chemically modified adsorbents. During the first experiment, an amount of cationic MB was placed in a test tube in a proportion of 10 g of each adsorbent/L of dye. According to the results (Figure 6a), the decrease in MB adsorption on the materials follows the order OL50M50C < OL50M50A < CL80OL10M10A < CL80OL10M10C ≈ CL80OL20A < CL80OL20C. The results show that the materials with a high proportion of zeolite (80%), i.e., CL80OL20C, CL80OL10M10C, CL80OL20A and CL80OL10M10A, have a maximum percentage of MB adsorption of more than 99% after 2 to 5 min, while OL50M50C and OL50M50A, which contain molasses and olive stone (50–50% *w*/*w*), reach an equilibrium after 30 and 10 min, respectively. Consequently, the carbonized material CL80OL20C, which consists of 80/20% *w*/*w* clinoptilolite/olive stone, adsorbs quicker (up to 2 min) and with higher amounts of MB dye in comparison with all the other materials.



(**a**) (**b**)

Figure 6. Adsorption percentage and adsorbed amount of (**a**) MB and (**b**) MR per g of material from aqueous solutions in carbonized and chemically modified materials.

Synthetic dyes can also be removed using activated carbons derived from olive industry by-products with great success. In order to be more specific, methylene blue adsorption reaches equilibrium at room temperature in less than one hour [89]. In other research, olive stone-based activated carbons presented maximum adsorption of methylene blue dye of approximately 1.2 mg/g, reaching an equilibrium after 80 min [90]. Moreover, new research conducted in combination with carbonaceous materials with zeolites approved that the use of coal gangue-based zeolite granules in a fluidized bed showed that the adsorption of MB from aqueous solutions follows chemical absorption with an adsorption saturation of 0.44 g/g and an equilibrium uptake of 108.04 mg/g [88]. Another study examined the adsorption of MB on activated carbon/natural zeolite nanoadsorbents in a batch experiment. According to the results, the pseudo-second order model fit well with the experimental data, showing that chemisorption is the prevailing mechanism. The maximum AC500/NZ adsorption capacity for MB dye was equal to 51 mg/g at an initial concentration of 30 ppm [77]. Mesoporous carbons prepared by using acid- and alkaline-treated zeolite X as the template and furfuryl alcohol as carbon source were used to adsorb MB, showing that the maximum adsorption was reached at 223 and 380 mg/g, respectively, and the pseudo-second order kinetic model better describes the adsorption data [91].

The second experiment examines the adsorptive behavior of the six materials with an anionic dye, i.e., methyl red (MR). The conditions of the experiment are the same as the previous one. Figure 6b shows the plot of the adsorption percentage and the amount of MR adsorbed versus the time for the six materials. It is observed that the adsorption of MR on all materials reaches an equilibrium at higher times than that of MB (approximately 30 min). The adsorption capacity increases according to the following order: OL50M50A < OL50M50C < CL80OL10M10C < CL80OL10M10A < CL80OL20A ≈ CL80OL20C. The adsorptive behavior of the materials on MR is similar to that of MB. It seems that the materials with a high proportion of zeolite (80%), i.e., CL80OL20C, A4CL80OL20A, CL80OL10M10C and CL80OL10M10A, have a maximum percentage of MR adsorption up to 98.0% for CL80OL20C and CL80OL20A and 93.7% for CL80OL10M10C and CL80OL10M10A, while OL50M50C and OL50M50A, which contain molasses and olive stone (50–50% *w*/*w*), present an adsorption percentage of MR equal to 46.5 and 42.2%, respectively. The activated carbons derived from *Moringa oleifera* shells (PMOS), activated with $ZnCL_2$ and calcined at different temperatures, were used for the adsorption of methyl red from aqueous solutions [92]. According to the results, the maximum MR sorption capacity was equal to 28.67 mg/g at ambient temperature. The process used exothermic chemisorption, and the pseudo-first order kinetic model was found to be suitable for describing the adsorptive kinetics of all prepared activated carbons.

Another study [93] examined the MB and MR dye adsorption on activated carbons derived from the chemical activation of caraway seeds using three different activators: Na_2CO_3, K_2CO_3 and H_3PO_4. The activation with potassium carbonate led to activated carbons with the highest specific surface area developed and the greatest sorption capacity, i.e., 296 mg/g for methylene blue and 208 mg/g for methyl red sodium salt. The pseudo-second order kinetic model better described the adsorption rate for both dyes in carbons.

Four kinetic models were applied to explain the adsorption of dyes in carbonized and chemically modified materials: the pseudo-first order, the pseudo-second order, the intraparticle diffusion and the Elovich model. The mathematical equations of each model are described in Table 4.

Table 4. Mathematical expression of the four kinetic models applied to the experimental data of dyes in the adsorbents [54].

Model Name	Mathematical Expression
Pseudo-first order	$\log(q_e - q_t) = \log q_e - \frac{K_1 t}{2.303}$
Pseudo-second order	$\frac{t}{q_t} = \frac{1}{K_{SE} q_e^2} + \frac{t}{q_e}$
Intraparticle diffusion	$q_t = K_D\, t^{1/2} + Z$
Elovich model	$q_t = \frac{1}{p} \ln(mp) + \frac{1}{p} \ln t$

where q_e: adsorption at equilibrium ($mg \cdot g^{-1}$), q_t: adsorption of dye ($mg \cdot g^{-1}$) at any time, t (min), K_L: Pseudo-first-order rate constant (min^{-1}), K_{SE}: Pseudo-second order rate constant ($g \cdot mg^{-1} \cdot min^{-1}$) K_D: Intraparticle diffusion coefficient ($mg \cdot g \cdot min^{-1/2}$), Z: constant ($mg \cdot g^{-1}$) showing that adsorption is controlled by multiple processes, m: initial adsorption rate constant of the Elovich model ($mg \cdot g^{-1} \cdot min^{-1}$) p: Desorption rate constant of the Elovich model ($g \cdot mg^{-1}$).

The adsorption kinetic study provides information on the adsorption rate, the performance of the used adsorbent and the mass transfer mechanisms. The pseudo-first order, pseudo-second order and Elovich models indicate that the chemisorption phenomenon takes place, while the intraparticle diffusion model stands more for physical sorption. Additionally, the identification of the experimental data with the pseudo-first order model means that the initial adsorbate concentration is high and that the active sites on the adsorbent are confined. On the other hand, the pseudo-second model indicates that the initial adsorbate concentration is low and that the adsorbent is abundant with numerous active sites [94]. The Elovich model is more often used in order to describe the sorption of gases onto a solid surface. The basic assumptions of the Elovich model are that the activation energy increases with adsorption time and that the surface of the adsorbent is heterogeneous. Finally, intraparticle diffusion basically stands for the transfer of the adsorbate into the pores of the adsorbent and best describes this stage of adsorption [95].

The kinetic models were used to investigate the mechanism of dye adsorption in the materials. The experimental data were fit to each model so that the best-fit equation was selected based on the correlation coefficient factor, R^2. According to the results (Table 5), the adsorption of dyes on carbonized CL80OL20C, CL80OL10M10C and OL50M50C and chemically modified CL80OL20A, CL80OL10M10A and OL50M50A materials are best described by the pseudo-second order model. The pseudo-second order model shows that the adsorption process proceeds via chemisorption or is controlled by chemical reactions, as mentioned above [96]. The other models, i.e., the pseudo-first order, Elovich and intraparticle diffusion models, are not presented due to the low correlation coefficient factors during their application to the experimental adsorption data of MB and MR on the materials. Other studies, which have been reported above [77,91,93], have shown that the prevailing model that better describes the experimental adsorption data of MB and MR on carbons is the pseudo-second order model.

Table 5. Kinetic parameters of pseudo-second order model based on the adsorption of MB and MR on carbonaceous and chemically modified materials.

Adsorbed Dye	Samples	q_e (mgg^{-1})	K_{SE} ($gmg^{-1}min^{-1}$)	R^2
MB	CL80OL20C	3.03	1.98	1.00
	CL80OL10M10C	3.22	1.56	0.99
	OL50M50C	2.99	0.70	1.00
	CL80OL20A	3.65	0.47	0.99
	CL80OL10M10A	3.41	0.50	0.98
	OL50M50A	2.97	2.03	1.00
MR	CL80OL20C	3.32	0.09	0.99
	CL80OL10M10C	3.05	0.38	0.99
	OL50M50C	1.72	0.29	1.00
	CL80OL20A	3.19	0.18	0.99
	CL80OL10M10A	3.07	0.68	1.00
	OL50M50A	1.36	4.01	0.99

The third experiment was conducted using olive mill wastewater to examine the capacity of the materials to adsorb the phenolic compounds that are present in it. The proportion of adsorbent to adsorbate was equal to 10 g of each adsorbent/L of wastewater. The results show that the material CL80OL20A adsorbs the maximum amount of total phenols (159.8 mg/g) after 30 min, while CL80OL10M10A adsorbs the maximum amount of 170.9 mg/g after 60 min, respectively (Figure 7). Then, the materials continue to adsorb total phenols, i.e., at 120 min, but in lower amounts (53.3 and 66.0 mg/g for CL80OL20A and CL80OL10M10A, respectively). The concentration of total phenols in the solution increases after 120 min (explaining the low adsorption values of the materials) due either to the desorption behavior of the materials (especially zeolite) or the release of polyphenolic compounds from the adsorbents into the solution [97].

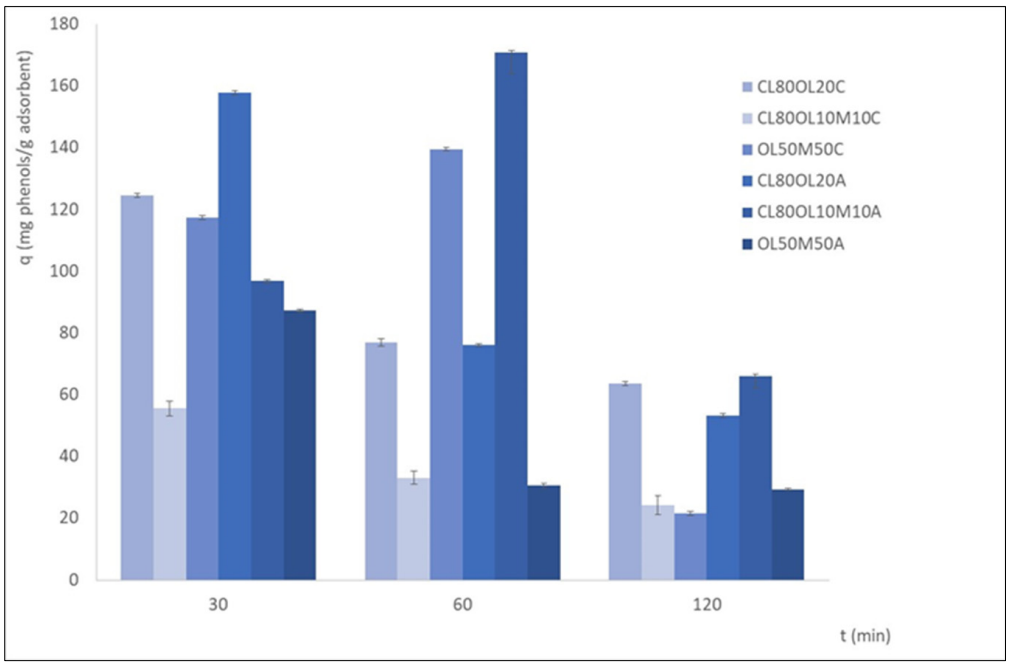


Figure 7. Adsorbed amount of total phenols per g of material from olive wastewater in carbonized and chemically modified materials.

The concentration of the desorbed phenolic compounds of each material in the deionized water versus time is presented in Figure 8. It seems that OL50M50A presents the highest desorption of phenolic compounds, equal to 264.2 mg/L, while the CL80OL10M10C material presents the lowest desorption, equal to 122.7 mg/L after 120 min. According to the results, the desorption process depends strongly on the type of raw materials and not the physical or chemical process. It seems that materials, which consist only of olive and sugarcane molasses (OL50M50A, OL50M50C) presented the highest phenolic desorption compared to materials with the highest percentage of clinoptilolite (CL80OL10M10C, CL80OL10M10A). Consequently, the adsorbents can be categorized into three groups: OL50M50A and OL50M50C (first group), CL80OL20A and CL80OL20C (second group) and CL80OL10M10A and CL80OL10M10C (third group) compared to phenolic compound desorption.

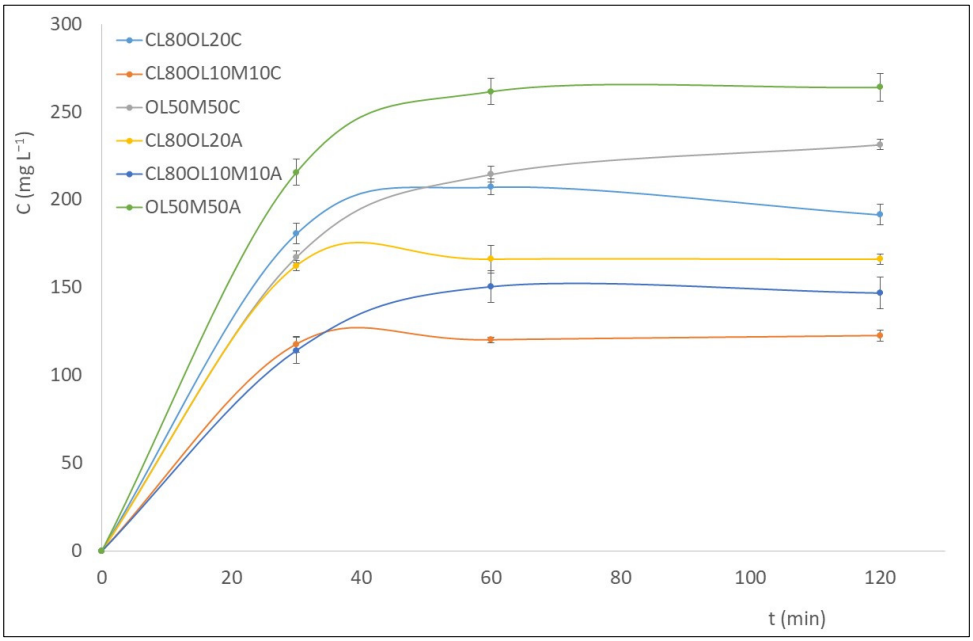


Figure 8. The concentration of the desorbed phenolic compounds of each material in the deionized water versus time.

After 120 min, the solutions were filtered to remove the adsorbents and the supernatant was added to falcon tubes with rice in a proportion of 0.1 g of rice/mL of supernatant. The adsorbed amount of the phenolic compounds from rice (mg of phenols/g of rice) after 60 min shows the following order: first solution (0.93 ± 0.03 mg/g) prepared by OL50M50A > second solution (0.74 ± 0.08 mg/g) prepared by CL80OL20C $\geq$ third solution (0.73 ± 0.03 mg/g) prepared by OL50M50C > fourth solution (0.54 ± 0.13 mg/g) prepared by CL80OL10M10A > fifth solution (0.41 ± 0.07 mg/g) prepared by CL80OL20A > sixth solution (0.14 ± 0.03 mg/g) prepared by CL80OL10M10C. It seems that the solution with the highest concentration of phenolic compounds (first group of adsorbents) leads to the highest adsorption of phenolics from rice. The adsorption–desorption method of phenolic compounds derived from olive mill wastewater provides an eco-friendly, sustainable, easy to apply and low-cost method to isolate bioactive molecules (phenols) and to add them into food, such as rice, to enrich it and to increase its content in these compounds. Phenols and sewage rich in it can cause severe environmental damage if they get discharged into it. By reclaiming phenolic compounds from industrial (olive mill) effluents, the environment and ecosystem are protected, while by using these compounds to enrich food, human health is promoted [98,99]. Consequently, this method provides an efficient way for the production of novel foods with high phenolic content.

Other studies have also used olive mill effluents as raw sources rich in bioactive compounds, like phenols. The isolation techniques that have been applied differ among studies, with extraction using chemical reagents such as acetone, to be the most common [100,101]. Therefore, adsorption is an efficient, low-cost and eco-friendly method, easy to apply. Studies that have used olive residues like olive stones to prepare activated carbons noted a phenol adsorption capacity of 58.8 mg/g after 60 min, while physiochemical activation generated activated carbons that reached total phenol adsorption of 158.7 mg/g after 24 h [102,103]. Commercial activated carbons such as coal-derived granular activated carbons, coal-derived powdered activated carbons and coconut shell-derived powdered activated carbons were used as adsorbents to study the effective removal of phenols from wastewater. The results show that the maximum adsorption capacity was 169.91, 176.58 and 212.96 mg/g for the three different commercial carbons. The chemically modified materials that were prepared in this current study by olive stones in addition to clinoptilolite and molasses (CL80OL20A and CL80OL10M10A) reached a maximum absorbance of phenols 166.8 mg/g after 60 min. The adsorption technique could be used not only to diminish the pollutant load of wastewater but can also be applied to make good use of the removed compounds. For instance, adsorption–desorption seems to be an efficient way of enriching food and drinks with bioactive compounds, such as phenols and antioxidants. This method has not been used extensively in these terms, so it is deemed to be a novel venture.

The adsorption of dyes and total phenols in the materials should be explained by the following factors: the specific surface area of adsorbents, the functional groups of adsorbents and adsorbates and the molecular structure of each adsorbate [104]. As it was mentioned previously, the specific surface area of each adsorbent follows the order OL50M50C < OL50M50A < CL80OL10M10C < CL80OL20C < CL80OL20A < CL80OL10M10A. Furthermore, the molecule of MB involves the aromatic rings, which include the functional groups of S^+ and $N^+(CH_3)_2$ (electron donors), while the molecule of MR presents the aromatic ring, which contains the functional groups of N=N, COOH (electron acceptors) and $N^+(CH_3)_2$ (electron donors) [105]. The molecule of phenol involves the aromatic ring of the phenol that acts as the electron acceptor [10,78]. These functional groups are responsible for electron donor–acceptor interactions between the functional groups of adsorbates and each carbonaceous or chemically modified material [105]. The functional groups of the materials were described in FTIR and RAMAN analysis, showing that the carbon coating on zeolitic surfaces led to high MR adsorption, i.e., CL80OL20C material up to 98% of MR adsorption, compared to zeolite itself (less than 20% of MR adsorption), as observed elsewhere [106]. This happens due to the negatively charged zeolitic surface, which repels the negative groups of MR, leading to low adsorption rates. Moreover, the different sizes of the molecules influence the adsorption process. MB and MR dyes present three and two aromatic rings in their molecules, respectively, indicating large molecules in diameter, which need materials with a mesopore structure in order to be adsorbed. Finally, the medium in which the adsorption takes place is also a factor that influences the whole process, i.e., the adsorption of dyes takes place in an aqueous solution, while the adsorption of total phenols in wastewater with other organic compounds may or may not facilitate the adsorption process.

4. Conclusions

New adsorbents were prepared by using by-products derived from the olive mill and sugar industry in combination with natural minerals, such as zeolite.

Regarding the characterization of the spectroscopic analysis of the materials: Raman spectroscopy presented two main characteristic bands in carbonaceous materials developed on zeolite, corresponding to G and D bands. Meanwhile, FTIR analysis showed absorption bands that corresponded to bending vibrations “in plane” of C–H or to Si–O bonds, out-of-plane alkenes (=C–H) or out-of-plane bending of ring C–H bonds and Si–O–AL bending vibrations.

Moreover, SEM analysis has shown that chemically modified adsorbents, i.e., CL80OL20A and CL80OL10M10A, appear to have a well-formed pore structure in comparison with carbonized ones, i.e., CL80OL10M10C and OL50M50C.

According to EDS analysis, the material CL80OL20C presents the highest ratio of C/O in EDS analysis and the lowest I_D/I_G in Raman spectroscopy.

Comparing the specific surface area (S_{bet}) of the materials, it seems that the increase in S_{bet} follows the order OL50M50C < OL50M50A < CL80OL10M10C < CL80OL20C < CL80OL20A < CL80OL10M10A. All samples show a type IV isotherm with a hysteresis loop, indicating mesoporous structures.

Regarding the batch experiments, the increase in the adsorption of MB or MR on materials follows the order: OL50M50C ≈ OL50M50A < CL80OL10M10A ≈ CL80OL10M10C < CL80OL20C ≈ CL80OL20A. According to the kinetic data, the well-fitted application of the pseudo-second order kinetic model to the experimental data has shown that chemisorption is the prevailing mechanism to both experiments. In addition, the adsorbed amount of the recovered phenols in rice range from 0.14 to 0.93 mg/g.

In conclusion, olive and sugar by-products can be transformed to filters either to adsorb dangerous organic compounds or to recover bioactive compounds from wastewater.

Author Contributions: Z.I. conceived the original idea, supervised the project and wrote the manuscript with support from C.M.G. C.M.G. contributed to the initial article research, methodology and data analysis and contributed to the interpretation of the Discussion Section. N.R. contributed to the experimental analysis and validation of the results. Z.I. and D.S. contributed to the final writing and corrections. All authors have read and agreed to the published version of the manuscript.

Funding: This present research was funded by EPAnEk-NRSF 2014–2020; the Operational Program "Competitiveness, Entrepreneurship and Innovation", Call 111 "Support of Regional Excellence" in the context of the implementation of the program AGRICA II: AGrifood Research and Innovation Network of ExCellence of the Aegean, which is co-financed by the European Regional Development Fund (ERDF), MIS code: 5046750.

Institutional Review Board Statement: This work does not contain any studies with human participants or animals.

Informed Consent Statement: All authors provided informed consent to participate in this research study.

Data Availability Statement: The datasets used and analyzed during this current study are available within the article, and the data presented in this study are available on request from the corresponding author.

Acknowledgments: The authors express their gratitude to Chrysoula Athanasekou (NCSR Demokritos) for the elemental composition analysis of the specimens.

Conflicts of Interest: The authors declare no conflict of interest.

References

1. Otero, P.; Garcia-Oliveira, P.; Carpena, M.; Barral-Martinez, M.; Chamorro, F.; Echave, J.; Garcia-Perez, P.; Cao, H.; Xiao, J.; Simal-Gandara, J.; et al. Applications of by-products from the olive oil processing: Revalorization strategies based on target molecules and green extraction technologies. *Trends Food Sci. Technol.* **2021**, *116*, 1084–1104. [CrossRef]
2. Contreras, M.D.M.; Romero, I.; Moya, M.; Castro, E. Olive-derived biomass as a renewable source of value-added products. *Process Biochem.* **2020**, *97*, 43–56. [CrossRef]
3. Al-Shaweesh, M.; Mohammed, M.; Al-Kabariti, D.; Khamash, D.; Al-Zawaidah, S.; Hindiyeh, M.; Omar, W. Olive mill wastewater (OMW) treatment by using ferric oxide dephenolization and chemical oxygen demand removal. *Glob. Nest J.* **2018**, *20*, 558–563. [CrossRef]
4. Chouchene, A.; Jeguirim, M.; Trouvé, G.; Favre-Reguillon, A.; Le Buzit, G. Combined process for the treatment of olive oil mill wastewater: Absorption on sawdust and combustion of the impregnated sawdust. *Bioresour. Technol.* **2010**, *101*, 6962–6971. [CrossRef]
5. Anastopoulos, I.; Bhatnagar, A.; Hameed, B.H.; Ok, Y.S.; Omirou, M. A review on waste-derived adsorbents from sugar industry for pollutant removal in water and wastewater. *J. Mol. Liq.* **2017**, *240*, 179–188. [CrossRef]

6. Raza, Q.-U.-A.; Bashir, M.A.; Rehim, A.; Sial, M.U.; Raza, H.M.A.; Atif, H.M.; Brito, A.F.; Geng, Y. Sugarcane industrial byproducts as challenges to environmental safety and their remedies: A review. *Water* **2021**, *13*, 3495. [CrossRef]
7. Sahu, O. Assessment of sugarcane industry: Suitability for production, consumption and utilization. *Ann. Agrar. Sci.* **2018**, *16*, 389–395. [CrossRef]
8. Kumar, A.; Kumar, S.; Kumar, S.; Gupta, D. Adsorption of phenol and 4-nitrophenol on granular activated carbon in basal salt medium: Equilibrium and kinetics. *J. Hazard. Mater.* **2007**, *147*, 155–166. [CrossRef]
9. Ahmaruzzaman, M.; Sharma, D.K. Adsorption of phenols from wastewater. *J. Colloid Interface Sci.* **2005**, *287*, 14–24. [CrossRef]
10. Dabrowski, A.; Podkoscielny, P.; Hubicki, Z.; Barczak, M. Adsorption of phenolic compounds by activated carbon—A critical review. *Chemosphere* **2005**, *58*, 1049–1070. [CrossRef]
11. Gomez, L.D.; Clare, G.S.; McQueen-Mason, J. Sustainable liquid biofuels from biomass: The writing's on the walls. *New Phytol.* **2008**, *178*, 473–485. [CrossRef] [PubMed]
12. Liao, Q.; Sun, J.; Gao, L. The adsorption of resorcinol from water using multiwalled carbon nanotubes. *Colloids Surf. A Physicochem. Eng. Asp.* **2008**, *312*, 160–165. [CrossRef]
13. Sun, Y.; Chen, J.; Li, A.; Liu, F.; Zhang, Q. Adsorption of resorcinol and catechol from aqueous solution by aminated hypercrosslinked polymers. *React. Funct. Polym.* **2005**, *64*, 63–73. [CrossRef]
14. Stoeckli, F.; López-Ramón, M.V.; Moreno-Castilla, C. Adsorption of phenolic compounds from aqueous solutions, by activated carbons, described by the Dubinin-Astakhov equation. *Langmuir* **2001**, *17*, 3301–3306. [CrossRef]
15. Caetano, M.; Valderrama, C.; Farran, A.; Cortina, J.L. Phenol removal from aqueous solution by adsorption and ion exchange mechanisms onto polymeric resins. *J. Colloid Interface Sci.* **2009**, *338*, 402–409. [CrossRef]
16. Al-Muhtaseb, A.H.; Ibrahim, K.A.; Albadarin, A.B.; Ali-khashman, O.; Walker, G.M.; Ahmad, M.N.M. Remediation of phenol-contaminated water by adsorption using poly(methyl methacrylate) (PMMA). *Chem. Eng. J.* **2011**, *168*, 691–699. [CrossRef]
17. Damjanovic, L.; Rakic, V.; Rac, V.; Auroux, D.S.A. The investigation of phenol removal from aqueous solutions by zeolites as solid adsorbents. *J. Hazard. Mater.* **2010**, *184*, 477–484. [CrossRef]
18. Li, L.; Quinlivan, P.A.; Knappe, D.R.U. Effects of activated carbon surface chemistry and pore structure on the adsorption of organic contaminants from aqueous solution. *Carbon* **2002**, *40*, 2085–2100. [CrossRef]
19. Alam, M.Z.; Ameem, E.S.; Muyibi, S.A.; Kabbashi, N.A. The factors affecting the performance of activated carbon prepared from oil palm empty fruit bunches for adsorption of phenol. *Chem. Eng. J.* **2009**, *155*, 191–198. [CrossRef]
20. Tsoncheva, T.; Mileva, A.; Tsyntsarski, B.; Paneva, D.; Spassova, I.; Kovacheva, D.; Velinov, N.; Karashanova, D.; Georgieva, B.; Petrov, N. Activated carbon from Bulgarian peach stones as a support of catalysts for methanol decomposition. *Biomass Bioenergy* **2018**, *109*, 135–146. [CrossRef]
21. Hazzaa, R.; Hussein, M. Adsorption of cationic dye from aqueous solution onto activated carbon prepared from olive stones. *Environ. Technol. Innov.* **2015**, *4*, 36–51. [CrossRef]
22. Rashidi, N.A.; Yusup, S. Potential of palm kernel shell as activated carbon precursors through single stage activation technique for carbon dioxide adsorption. *J. Clean. Prod.* **2017**, *168*, 474–486. [CrossRef]
23. Sun, Y.; Li, H.; Li, G.; Gao, B.; Yue, Q.; Li, X. Characterization and ciprofloxacin adsorption properties of activated carbons prepared from biomass wastes by H_3PO_4 activation. *Bioresour. Technol.* **2016**, *217*, 239–244. [CrossRef]
24. Zhang, D.; Huo, P.; Liu, W. Behavior of phenol adsorption on thermal modified activated carbon. *Chin. J. Chem. Eng.* **2016**, *24*, 446–452. [CrossRef]
25. Zubrik, A.; Matik, M.; Hredzák, S.; Lovás, M.; Danková, Z.; Kováčová, M.; Briančin, J. Preparation of chemically activated carbon from waste biomass by single-stage and two-stage pyrolysis. *J. Clean. Prod.* **2017**, *143*, 643–653. [CrossRef]
26. Kumar, U.; Maroufi, S.; Rajarao, R.; Mayyas, M.; Mansuri, I.; Joshi, R.K.; Sahajwalla, V. Cleaner production of iron by using waste macadamia biomass as a carbon resource. *J. Clean. Prod.* **2017**, *158*, 218–224. [CrossRef]
27. Enniya, I.; Rghioui, L.; Jourani, A. Adsorption of hexavalent chromium in aqueous solution on activated carbon prepared from apple peels. *Sustain. Chem. Pharm.* **2018**, *7*, 9–16. [CrossRef]
28. Menya, E.; Olupot, P.W.; Storz, H.; Lubwama, M.; Kiros, Y. Production and performance of activated carbon from rice husks for removal of natural organic matter from water: A review. *Chem. Eng. Res. Des.* **2018**, *129*, 271–296. [CrossRef]
29. Tsoncheva, T.; Velinov, N.; Ivanova, R.; Stoycheva, I.; Tsyntsarski, B.; Spassova, I.; Paneva, D.; Issa, G.; Kovacheva, D.; Genova, I.; et al. Formation of catalytic active sites in iron modified activated carbons from agricultural residues. *Microporous Mesoporous Mater.* **2015**, *217*, 87–95. [CrossRef]
30. Fiuza, R.A., Jr.; Medeiros de Jesus Neto, R.; Correia, L.B.; Carvalho Andrade, H.M. Preparation of granular activated carbons from yellow mombin fruit stones for CO_2 adsorption. *J. Environ. Manag.* **2015**, *161*, 196–205. [CrossRef]
31. Alabadi, A.; Razzaque, S.; Yang, Y.; Chen, S.; Tan, B. Highly porous activated carbon materials from carbonized biomass with high CO_2 capturing capacity. *Chem. Eng. J.* **2015**, *281*, 606–612. [CrossRef]
32. Ribeiro, R.F.L.; Soares, V.C.; Costa, L.M.; Nascentes, C.C. Production of activated carbon from biodiesel residues: An alternative for hazardous metal sorption from aqueous solutions. *J. Environ. Manag.* **2015**, *162*, 123–131. [CrossRef] [PubMed]
33. Wang, Y.X.; Ngo, H.H.; Guo, W.S. Preparation of a specific bamboo based activated carbon and its application for ciprofloxacin removal. *Sci. Total Environ.* **2015**, *533*, 32–39. [CrossRef] [PubMed]
34. Zhang, Y.-J.; Ou, J.-L.; Duan, Z.K.; Xing, Z.J.; Wang, Y. Adsorption of Cr(VI) on bamboo bark-based activated carbon in the absence and presence of humic acid. *Colloids Surf. A Physicochem. Eng. Asp.* **2015**, *481*, 108–116. [CrossRef]

35. Rafatullaha, M.; Sulaimana, O.; Hashima, R.; Ahmad, A. Adsorption of methylene blue on low-cost adsorbents: A review. *J. Hazard. Mater.* **2010**, *177*, 70–80. [CrossRef]
36. Capobianco, L.; Di Caprio, F.; Altimari, P.; Astolfi, M.L.; Pagnanelli, F. Production of an iron-coated adsorbent for arsenic removal by hydrothermal carbonization of olive pomace: Effect of the feedwater pH. *J. Environ. Manag.* **2020**, *273*, 111164. [CrossRef]
37. Gao, Y.; Yue, Q.; Gao, B.; Li, A. Insight into activated carbon from different kinds of chemical activating agents: A review. *Sci. Total Environ.* **2020**, *746*, 141094. [CrossRef]
38. Pietrzak, R.; Nowicki, P.; Kaźmierczak, J.; Kuszyńska, I.; Goscianska, J.; Przepiórski, J. Comparison of the effects of different chemical activation methods on properties of carbonaceous adsorbents obtained from cherry stones. *Chem. Eng. Res. Des.* **2014**, *92*, 1187–1191. [CrossRef]
39. Brito, M.J.P.; Veloso, C.M.; Santos, L.S.; Bonomo, R.C.F.; Fontan, R.D.C.I. Adsorption of the textile dye Dianix® royal blue CC onto carbons obtained from yellow mombin fruit stones and activated with KOH and H_3PO_4: Kinetics, adsorption equilibrium and thermodynamic studies. *Powder Technol.* **2018**, *339*, 334–343. [CrossRef]
40. Özsin, G.; Pütün, A.E. TGA/MS/FT-IR study for kinetic evaluation and evolved gas analysis of a biomass/PVC co-pyrolysis process. *Energy Convers. Manag.* **2019**, *182*, 143–153. [CrossRef]
41. Mahmoud, A.; Ahmed, E. Biomass Carbonization, chapter 11. In *Renewable Energy—Resources, Challenges and Applications*; Al Qubeissi, M., El-kharouf, A., Soyhan., H.S., Eds.; Knowledge Unlatched: London, UK, 2020; pp. 211–233, ISBN 978-1-78984-284-5.
42. Sevilla, M.; Mokaya, R. Energy storage applications of activated carbons: Supercapacitors and hydrogen storage. *Energy Environ. Sci.* **2014**, *7*, 1250–1280. [CrossRef]
43. Kordala, N.; Wyszkowski, M. Zeolite Properties, Methods of Synthesis, and Selected Applications. *Molecules* **2024**, *29*, 1069. [CrossRef] [PubMed]
44. Moshoeshoe, M.; Nadiye-Tabbiruka, M.S.; Obuseng, V. A Review of the Chemistry, Structure, Properties and Applications of Zeolites. *Am. J. Mater. Sci.* **2017**, *7*, 196–221.
45. Kakhki, R.M.; Zirjanizadeh, S.; Mohammadpoor, M. A review of clinoptilolite, its photocatalytic, chemical activity, structure and properties: In time of artificial intelligence. *J. Mater Sci.* **2023**, *58*, 10555–10575. [CrossRef]
46. Ioannou, Z.; Dimirkou, A.; Golia, E.; Ioannou, A. Sorption of Zn by clinoptilolite-Fe$(NO_3)_3$ systems. *Commun. Soil Sci. Plant Anal.* **2009**, *40*, 240–258. [CrossRef]
47. *ISO 11465*; Soil Quality—Determination of Dry Matter and Water Content on a Mass Basis—Gravimetric Method. International Organization for Standardization: Geneva, Switzerland, 1993.
48. Jones, J.B.; Case, V.W. Sampling, handling and analyzing plant tissue samples. In *Soil Testing and Plant Analysis*, 3rd ed.; Westerman, R.L., Ed.; Book Series No. 3; Soil Science Society of America: Madison, WI, USA, 1990; pp. 389–427.
49. *EN 15148*; Solid Biofuels—Determination of the Content of Volatile Matter. European Committee for Standardization: Brussels, Belgium, 2009.
50. Kwaghger, A.; Ibrahim, J.S. Optimization of Conditions for the Preparation of Activated Carbon from Mango Nuts Using HCL. *Am. J. Eng. Res.* **2013**, *7*, 74–85.
51. Ma, J.; Tan, L.; Xie, S.; Feng, Y.; Shi, Z.; Ke, S.; He, Q.; Ke, Q.; Zhao, Q. The role of hydrochloric acid pretreated activated carbon in chain elongation of D-lactate to caproate: Adsorption and facilitation. *Environ. Res.* **2023**, *233*, 116387. [CrossRef] [PubMed]
52. Aslan, S.; Sirazi, M. Adsorption of Sulfonamide Antibiotic onto Activated Carbon Prepared from an Agro-industrial By-Product as Low-Cost Adsorbent: Equilibrium, Thermodynamic, and Kinetic Studies. *Water Air Soil Pollut.* **2020**, *231*, 222. [CrossRef]
53. Aziz, H.A.; Lee, W.J.; Ibrahim, N. Removal of Coliform, Suspended Solids, UV254 and Colour Using Zeolite and Activated Carbon in Riverbank Filtration System. *Int. J. Eng.* **2020**, *33*, 732–736.
54. Itodo, A.U.; Abdulrahman, F.W.; Hassan, L.G.; Maigandi, S.A.; Itodo, H.U. Physicochemical parameters of Adsorbents from locally sorted H3PO4 and ZnCl2 modified Agricultural wastes. *N. Y. Sci. J.* **2010**, *3*, 17–24.
55. Saka, C. BET, TG–DTG, FT-IR, SEM, iodine number analysis and preparation of activated carbon from acorn shell by chemical activation with ZnCl2. *Turk. J. Anal. Appl. Pyrolysis* **2012**, *95*, 21–24. [CrossRef]
56. Ioannou, Z.; Simitzis, J. Adsorption kinetics of phenol and 3-nitrophenol from aqueous solutions on conventional and novel carbons. *J. Hazard. Mater.* **2009**, *171*, 954–964. [CrossRef] [PubMed]
57. Ioannou, Z.; Simitzis, J. Production of carbonaceous adsorbents from agricultural by-products and novolac resin under a continuous countercurrent flow type pyrolysis operation. *Bioresour. Technol.* **2013**, *129*, 191199. [CrossRef]
58. Wang, S.; Dou, J.; Zhang, T.; Li, S.; Chen, X. Selective adsorption of Methyl Orange and Methylene Blue by porous carbon material prepared from potassium citrate. *ACS Omega* **2023**, *8*, 35024–35033. [CrossRef]
59. Box, J.D. Investigation of the Folin-Ciocalteau phenol reagent for the determination of polyphenolic substances in natural waters. *Water Res.* **1983**, *17*, 511–525. [CrossRef]
60. Krichene, D.; Salvador, M.D.; Fregapane, G. Stability of Virgin Olive Oil Phenolic Compounds during Long-Term Storage (18 Months) at Temperatures of 5−50 °C. *J. Agric. Food Chem.* **2015**, *63*, 6779–6786. [CrossRef] [PubMed]
61. Papaoikonomou, L.; Labanaris, K.; Kaderides, K.; Goula, A.M. Adsorption–desorption of phe-nolic compounds from olive mill wastewater using a novel low-cost biosorbent. *Environ. Sci. Pollut. Res.* **2021**, *28*, 24230–24244. [CrossRef]
62. Dirbeba, M.J.; Brink, A.; Lindberg, D.; Hupa, M.; Hupa, L. Thermal Conversion Characteristics of Molasses. *ACS Omega* **2021**, *6*, 21631–21645. [CrossRef]

63. Castells, B.; Varela, A.; Castillo-Ruiz, F.J.; Calvo, L.F.; Medic, L.; Tascón, A. Ignition and explo-sion characteristics of olive-derived biomasses. *Powder Technol.* **2023**, *420*, 118386. [CrossRef]
64. Pabiś-Mazgaj, E.; Gawenda, T.; Pichniarczyk, P.; Stempkowska, A. Mineral Composition and Structural Characterization of the Clinoptilolite Powders Obtained from Zeolite-Rich Tuffs. *Minerals* **2021**, *11*, 1030. [CrossRef]
65. Ibrahim, J.E.F.M.; Apkarian, A.S.; Tihtih, M.; Kulkov, S.N.; Gomze, L.A. In-situ carbonization of natural zeolite-alumina composite materials incorporated sawdust. *J. Silic. Based Compos. Mater.* **2021**, *73*, 137–144. [CrossRef]
66. Yoshida, A.; Kaburagi, Y.; Hishiyama, Y. Full width at half maximum intensity of the G band in the first order Raman spectrum of carbon material as a parameter for graphitization. *Carbon* **2006**, *44*, 2333–2335. [CrossRef]
67. Kwiecinska, B.; Suárez-Ruiz, I.; Paluszkiewicz, C.; Rodriques, S. Raman spectroscopy of selected carbonaceous samples. *Int. J. Coal Geol.* **2010**, *84*, 206–212. [CrossRef]
68. Ferrari, A.C.; Robertson, J. Interpretation of Raman spectra of disordered and amorphous carbon. *Phys. Rev. B* **2000**, *61*, 14095. [CrossRef]
69. Finocchiaro, C.; Coccato, A.; Barone, G.; Bersani, D.; Culka, A.; Fornasini, L.; Mazzoleni, P.; Jehlička, J.; Rousaki, A.; Vandenabeele, P. In situ and micro-Raman spectroscopy for the identification of natural Sicilian zeolites. *J. Raman Spectrosc.* **2022**, *53*, 525–539. [CrossRef]
70. Wang, Y.; Alsmeyer, D.C.; McCreery, R.L. Raman spectroscopy of carbon materials: Structural basis of observed spectra. *Chem. Mater.* **1990**, *2*, 557–563. [CrossRef]
71. Pyrzyńska, K.; Bystrzejewski, M. Comparative study of heavy metal ions sorption onto activated carbon, carbon nanotubes, and carbon-encapsulated magnetic nanoparticles. *Colloids Surf. A Physicochem. Eng. Asp.* **2010**, *362*, 102–109. [CrossRef]
72. Pang, H.; Wang, X.; Zhang, G.; Chen, H.; Lv, G.; Yang, S. Characterization of diamond-like carbon films by SEM, XRD and Raman spectroscopy. *Appl. Surf. Sci.* **2010**, *256*, 6403–6407. [CrossRef]
73. Li, Z.; Deng, L.; Kinloch, I.A.; Young, R.J. Raman spectroscopy of carbon materials and their composites: Graphene, nanotubes and fibers. *Prog. Mater. Sci.* **2023**, *135*, 101089. [CrossRef]
74. Knight, D.S.; White, W.B. Characterization of diamond films by Raman spectroscopy. *J. Mater. Res.* **1989**, *4*, 385–393. [CrossRef]
75. Ma, Y.K.; Rigolet, S.; Michelin, L.; Paillaud, J.L.; Mintova, S.; Khoerunnisa, F.; Daou, T.J.; Ng, E.P. Facile and fast determination of Si/Al ratio of zeolites using FTIR spectroscopy technique. *Microporous Mesoporous Mater.* **2021**, *311*, 110683. [CrossRef]
76. Yin, X.-M.; Xie, X.M.; Wu, X.; An, X. Catalytic performance of nickel immobilized on organically modified montmorillonite in the steam reforming of ethanol for hydrogen production. *J. Fuel Chem. Technol.* **2016**, *44*, 689–697. [CrossRef]
77. Mohamed, F.; Shaban, M.; Zaki, S.K.; Abd-Elsamie, M.S.; Sayed, R.; Zayed, M.; Khalid, N.; Saad, S.; Omar, S.; Ahmed, A.M.; et al. Activated carbon derived from sugarcane and modified with natural zeolite for efficient adsorption of methylene blue dye: Experimentally and theoretically approaches. *Sci. Rep.* **2022**, *12*, 18031. [CrossRef] [PubMed]
78. Xie, B.; Jihong, Q.; Wang, S.; Li, X.; Sun, H.; Chen, W. Adsorption of Phenol on Commercial Activated Carbons: Modelling and Interpretation. *Int. J. Environ. Res. Public Health* **2020**, *17*, 789. [CrossRef]
79. Sydorchuk, V.; Vasylechko, V.; Khyzhun, O.; Gryshchouk, G.; Khalameida, S.; Vasylechko, L. Effect of high-energy milling on the structure, some physicochemical and photocatalytic properties of clinoptilolite. *Appl. Catal. A Gen.* **2021**, *610*, 117930. [CrossRef]
80. Soukoulis, C.; Tzia, C. Grape, raisin and sugarcane molasses as potential partial sucrose substitutes in chocolate ice cream: A feasibility study. *Int. Dairy J.* **2018**, *76*, 18–29. [CrossRef]
81. Kacan, E. Optimum BET surface areas for activated carbon produced from textile sewage sludges and its application as dye removal. *J. Environ. Manag.* **2016**, *166*, 116–123. [CrossRef]
82. Kim, J.H.; Hwang, S.Y.; Park, J.E.; Lee, G.B.; Kim, H.; Kim, S.; Hong, B.U. Impact of the oxygen functional group of nitric acid-treated activated carbon on KOH activation reaction. *Carbon Lett.* **2019**, *29*, 281–287. [CrossRef]
83. Qiu, C.; Jiang, L.; Gao, Y.; Sheng, L. Effects of oxygen-containing functional groups on carbon materials in supercapacitors: A review. *Mater. Des.* **2023**, *230*, 1–33. [CrossRef]
84. Yang, S.Y.; Bai, B.C.; Kim, Y.R. Effective Surface Structure Changes and Characteristics of Activated Carbon with the Simple Introduction of Oxygen Functional Groups by Using Radiation Energy. *Surfaces* **2024**, *7*, 12–25. [CrossRef]
85. Everett, D.H. IUPAC, Manual of symbol and terminology for physico-chemical quantities and units, Appendix, Definitions, Terminology and Symbols in Colloid and Surface Chemistry. *Pure Appl. Chem.* **1972**, *31*, 577–638. [CrossRef]
86. Xu, L.; Zhang, J.; Ding, J.; Liu, T.; Shi, G.; Li, X.; Dang, W.; Cheng, Y.; Guo, R. Pore Structure and Fractal Characteristics of Different Shale Lithofacies in the Dalong Formation in the Western Area of the Lower Yangtze Platform. *Minerals* **2020**, *10*, 72. [CrossRef]
87. Taher, T.; Maulana, S.; Mawaddah, N.; Munandar, A.; Rianjanu, A.; Lesbani, A. Low-temperature hydrothermal carbonization of activated carbon microsphere derived from microcrystalline cellulose as carbon dioxide (CO_2) adsorbent. *Mater. Today Sustain.* **2023**, *23*, 100464. [CrossRef]
88. Lv, B.; Dong, B.; Zhang, C.; Chen, Z.; Zhao, Z.; Deng, X.; Fang, C. Effective adsorption of methylene blue from aqueous solution by coal gangue-based zeolite granules in a fluidized bed: Fluidization characteristics and continuous adsorption. *Powder Technol.* **2022**, *408*, 117764. [CrossRef]
89. Benzekri, B.M.; Benderdouche, N.; Bestani, B.; Douara, N.; Duclaux, L. Valorization of olive stones into a granular activated carbon for the removal of Methylene blue in batch and fixed bed modes. *J. Mater. Environ. Sci.* **2018**, *9*, 272–284. [CrossRef]
90. Berrios, M.; Martín, M.A.; Martín, A. Treatment of pollutants in wastewater: Adsorption of methylene blue onto olive-based activated carbon. *J. Ind. Eng. Chem.* **2012**, *18*, 780–784. [CrossRef]

91. Yan, C.; Wang, C.; Yao, J.; Zhang, L.; Liu, X. Adsorption of methylene blue on mesoporous carbons prepared using acid- and alkaline-treated zeolite X as the template. *Colloids Surf. A Physicochem. Eng. Asp.* **2009**, *333*, 115–119. [CrossRef]
92. Khalfaoui, A.; Bouchareb, E.M.; Derbal, K.; Boukhaloua, S.; Chahbouni, B.; Bouchare, R. Uptake of Methyl Red dye from aqueous solution using activated carbons prepared from *Moringa oleifera* shells. *Clean. Chem. Eng.* **2022**, *4*, 100069. [CrossRef]
93. Paluch, D.; Bazan-Wozniak, A.; Nosal-Wiercińska, A.; Pietrzak, R. Removal of Methylene Blue and Methyl Red from Aqueous Solutions Using Activated Carbons Obtained by Chemical Activation of Caraway Seed. *Molecules* **2023**, *28*, 6306. [CrossRef]
94. Wang, J.; Guo, X. Adsorption kinetic models: Physical meanings, applications, and solving methods. *J. Hazard. Mater.* **2020**, *390*, 122156. [CrossRef]
95. Wang, J.; Guo, X. Rethinking of the intraparticle diffusion adsorption kinetics model: Interpretation, solving methods and applications. *Chemosphere* **2022**, *309*, 136732. [CrossRef] [PubMed]
96. Khamizov, R.K. A Pseudo-Second Order Kinetic Equation for Sorption Processes. *Russ. J. Phys. Chem. A* **2020**, *94*, 171–176. [CrossRef]
97. Stasinakis, A.S.; Elia, I.; Petalas, A.V.; Halvadakis, C.P. Removal of total phenols from olive-mill wastewater using an agricultural by-product, olive pomace. *J. Hazard. Mater.* **2008**, *160*, 408–413. [CrossRef] [PubMed]
98. Athanasiadis, V.; Voulgaris, A.; Katsoulis, K.; Lalas, S.I.; Roussis, I.G.; Gortzi, O. Development of Enriched Oil with Polyphenols Extracted from Olive Mill Wastewater. *Foods* **2023**, *12*, 497. [CrossRef]
99. Ziati, M.; Khemmari, F.; Cherifi, O.; Didouche, F.Y. Removal of polyphenols from olive mill wastewater by adsorption on activated carbon prepared from each stones. *Acad. Romana* **2017**, *62*, 865–874.
100. Caporaso, N.; Formisano, D.; Genovese, A. Use of phenolic compounds from olive mill wastewater as valuable ingredients for functional foods. *Crit. Rev. Food Sci. Nutr.* **2018**, *58*, 2829–2841. [CrossRef]
101. Skaltsounis, A.L.; Argyropoulou, A.; Aligiannis, N.; Xynos, N. Recovery of High Added Value Compounds from Olive Tree Products and Olive Processing Byproducts. In *Olive and Olive Oil Bioactive Constituents*; AOCS Press: Champaign, IL, USA, 2015; pp. 333–356. [CrossRef]
102. Bohli, T.; Fiol, N.; Villaescusa, I.; Ouedern, A. Adsorption on Activated Carbon from Olive Stones: Kinetics and Equilibrium of Phenol Removal from Aqueous Solution. *Chem. Eng. Process Technol.* **2013**, *4*, 165. [CrossRef]
103. Temdrara, L.; Addoun, A.; Khelifi, A. Development of olivestones-activated carbons by physical, chemical and physicochemical methods for phenol removal: A comparative study. *Desalination Water Treat.* **2015**, *53*, 452–461. [CrossRef]
104. El Hanandeh, A.; Albalasmeh, A.; Gharaibeh, M.; Alajlouni, M. Modification of biochar prepared from olive oil processing waste to enhance phenol removal from synthetic and olive mill wastewater. *Sep. Sci. Technol.* **2020**, *56*, 1–13. [CrossRef]
105. Simitzis, J.; Ioannou, Z. Activated Carbonaceous Materials Based on Thermosetting Binder Precursors. In *Activated Carbon: Classifications, Properties and Applications*; Kwiatkowski, J.F., Ed.; Nova Publishing Inc.: Hauppauge, NY, USA, 2011; pp. 377–392.
106. Ioannou, Z.; Karasavvidis, C.; Dimirkou, A.; Antoniadis, A. Adsorption of methylene blue and methyl red dyes from aqueous solutions onto modified zeolites. *Water Sci. Technol.* **2013**, *67*, 1129–1136. [CrossRef]

Disclaimer/Publisher's Note: The statements, opinions and data contained in all publications are solely those of the individual author(s) and contributor(s) and not of MDPI and/or the editor(s). MDPI and/or the editor(s) disclaim responsibility for any injury to people or property resulting from any ideas, methods, instructions or products referred to in the content.